JGR Solid Earth

RESEARCH ARTICLE
10.1029/2023JB027965

Mantle Structure Beneath the Damara Belt in South-Central Africa Imaged Using Adaptively Parameterized P-Wave Tomography

Hesam Saeidi[1], Samantha E. Hansen[1], Andrew A. Nyblade[2,3], and Ryan Haag[1]

[1]Geological Sciences Department, The University of Alabama, Tuscaloosa, AL, USA, [2]Geosciences Department, The Pennsylvania State University, University Park, PA, USA, [3]School of Geosciences, University of the Witwatersrand, Johannesburg, South Africa

Key Points:

- New P-wave tomography model highlights the structure of the Large Low Velocity Province beneath south-central Africa
- Anomalously slow seismic velocities beneath the Damara Belt are constrained to depths below ~1,200 km
- Slow velocities ascend to the northeast, crossing into the upper mantle beneath the Irumide Belt and the East African Rift System

Supporting Information:

Supporting Information may be found in the online version of this article.

Correspondence to:

H. Saeidi,
hsaeidi@crimson.ua.edu

Citation:

Saeidi, H., Hansen, S. E., Nyblade, A. A., & Haag, R. (2024). Mantle structure beneath the Damara Belt in south-central Africa imaged using adaptively parameterized P-wave tomography. *Journal of Geophysical Research: Solid Earth*, *129*, e2023JB027965. https://doi.org/10.1029/2023JB027965

Received 28 SEP 2023
Accepted 10 FEB 2024

Author Contributions:

Conceptualization: Hesam Saeidi, Samantha E. Hansen, Andrew A. Nyblade
Data curation: Hesam Saeidi, Ryan Haag
Formal analysis: Hesam Saeidi
Funding acquisition: Samantha E. Hansen, Andrew A. Nyblade
Investigation: Hesam Saeidi
Methodology: Hesam Saeidi, Samantha E. Hansen
Project administration: Samantha E. Hansen
Resources: Hesam Saeidi
Software: Hesam Saeidi
Supervision: Samantha E. Hansen
Validation: Hesam Saeidi, Andrew A. Nyblade
Visualization: Hesam Saeidi, Samantha E. Hansen
Writing – original draft: Hesam Saeidi

Abstract Many seismic tomography studies have indicated that the African Large Low Velocity Province (LLVP) extends from the lower mantle beneath southern Africa into the upper mantle beneath eastern Africa; however, it has been questioned whether the LLVP structure may also extend to the north or northwest beneath south-central Africa. Debates regarding the upper mantle structure beneath the Damara Belt contribute to this uncertainty. Some studies suggest the Damara Belt is underlain by thermally perturbed upper mantle; however, other studies indicate the region is not associated with anomalous structure. Here, we use a comprehensive P-wave travel-time data set and an adaptive model parameterization to develop a new tomographic model for the Damara Belt and surrounding regions. Our results show that seismically slow structure beneath the Damara Belt is relegated to depths greater than ~1,200 km, indicating that the LLVP is not significantly affecting this region. However, further to the northeast, the LLVP structure obliquely rises and crosses the mantle transition zone near the Irumide Belt, where it then extends into the upper mantle. The seismic structure beneath the Damara Belt and neighboring areas in our model correlates well with tectonic observations at the surface, including variations in heat flow, the distribution of geothermal features, the locations of rifts, and estimates of dynamic topography.

Plain Language Summary The African Large Low Velocity Province (LLVP) is an anomalous feature in the Earth's mantle, thought to be associated with unique temperature and compositional characteristics. Many prior studies have shown that the LLVP originates near the core-mantle boundary beneath southern Africa but then ascends to the northeast, reaching the upper part of the mantle beneath eastern Africa. However, it is unclear whether the LLVP also extends to the north or northwest beneath the Damara Belt in south-central Africa. Using the travel-times of earthquake signals recorded by stations across the continent, we have created a new model of the seismic velocity structure beneath south-central Africa, which can be interpreted in terms of thermal and compositional variations. Slow velocities associated with the LLVP are constrained to depths greater than ~1,200 km beneath the Damara Belt, which indicates that the LLVP has little affect on this region. However, the slow LLVP structure rises to the northeast, moving into the upper mantle beneath the Irumide Belt and the East African Rift System. The trend of the LLVP structure in our model well matches various features observed at the surface.

1. Introduction

The Large Low Velocity Province (LLVP) beneath southern Africa is a first-order, lower mantle feature that was initially imaged by seismic tomography studies more than 30 years ago (e.g., Dziewonski & Anderson, 1984; Kárason & van der Hilst, 2000; Ni et al., 2002; Ni & Helmberger, 2003; Ritsema et al., 1999; Sleep et al., 2002). As new seismic data sets, particularly from southern and eastern Africa (Benoit, Nyblade, Owens, & Stuart, 2006, Benoit, Nyblade, & VanDecar, 2006; Fishwick, 2010; Fonseca et al., 2014; Montelli et al., 2004, 2006; Nyblade et al., 2008; Ritsema et al., 1998; Yuan & Li, 2022), have become available, our understanding of the LLVP's origin, composition, and how high it rises above the core-mantle boundary (CMB) have improved. Many tomographic models show that the LLVP extends from the lower mantle beneath southern Africa to the northeast, crossing into the upper mantle beneath eastern Africa (e.g., Celli et al., 2020; Chorowicz, 2005; Corti, 2009; Hansen et al., 2012; Hansen & Nyblade, 2013), and it has been suggested that continental rifting in the East African Rift System (EARS) is driven by the ascending LLVP structure (Boyce et al., 2021; Chang et al., 2020; Hansen et al., 2012; Hansen & Nyblade, 2013; Rajaonarison et al., 2023). However, existing tomographic images have limited resolution of the mantle structure beneath south-central Africa, which has led to questions about

Writing – review & editing:
Hesam Saeidi, Samantha E. Hansen, Andrew A. Nyblade

whether the LLVP structure also extends to the north or northwest. In particular, there have been disagreements regarding the upper mantle structure beneath the Neoproterozoic Damara Belt, a tectonic region that is situated between the Congo and Kalahari cratons (Figure 1). Some prior studies advocate for a seismically slow upper mantle beneath this area (e.g., Akinremi et al., 2022; Begg et al., 2009; Ortiz et al., 2019; Yu, Gao, et al., 2015, 2017), which could possibly indicate an extension of the African LLVP into the upper mantle beneath south-central Africa. Conversely, others have argued that there is no evidence for anomalously slow mantle beneath the Damara Belt (e.g., Afonso et al., 2022; Celli et al., 2020; Pandey et al., 2022; Priestley et al., 2008; White-Gaynor et al., 2020, 2021); rather, the lithosphere in this region may just be thin compared to the thick lithosphere beneath the surrounding cratons (Afonso et al., 2022; White-Gaynor et al., 2020, 2021).

To further investigate the tectonic structure beneath the Damara Belt and neighboring regions, we have combined an adaptively parameterized teleseismic P-wave tomography approach with new seismic data to generate a high-resolution 3-D image of the mantle beneath south-central Africa. This technique benefits from comprehensive seismic ray path coverage of the entire mantle beneath the African continent as it combines data from both a global catalog as well as from regional networks (Boyce et al., 2021; Hansen et al., 2012; Hansen & Nyblade, 2013; Kárason & van der Hilst, 2000; Saeidi et al., 2023; Weston et al., 2018). We aim to determine whether the upper mantle beneath the study area shows evidence for thermal perturbation and if so, to determine whether this anomalous structure is associated with the African LLVP. Further, we seek to determine whether the mantle structure beneath south-central Africa may directly influence surface features, such as geothermal activity and continental rifting.

2. Geologic Background and Previous Studies

The tectonic terranes in south-central Africa primarily consist of Archean cratons surrounded by Proterozoic mobile belts (Figure 1). The Kaapvaal and Zimbabwe Cratons, which formed between about 3.2 and 2.5 Ga, are joined by the Neoarchean Limpopo mobile belt, and collectively these terranes are known as the Kalahari Craton. The Congo Craton formed at about the same time and is composed of various Archean and Proterozoic blocks. Between about 2.5 and 1.6 Ga, the Rehoboth Province and the Kheis Belt were accreted to the western edge of the Kaapvaal Craton, and later (about 1.2–1.0 Ga) the Namaqua-Natal mobile belt developed along the southern boundary of the craton. The Irumide Belt, north of the Zimbabwe Craton (Figure 1), also formed at about the same time as the Namaqua-Natal Belt (Begg et al., 2009; Chorowicz, 2005; De Waele et al., 2006; de Wit et al., 1992; Johnson et al., 2005; Miller et al., 2009).

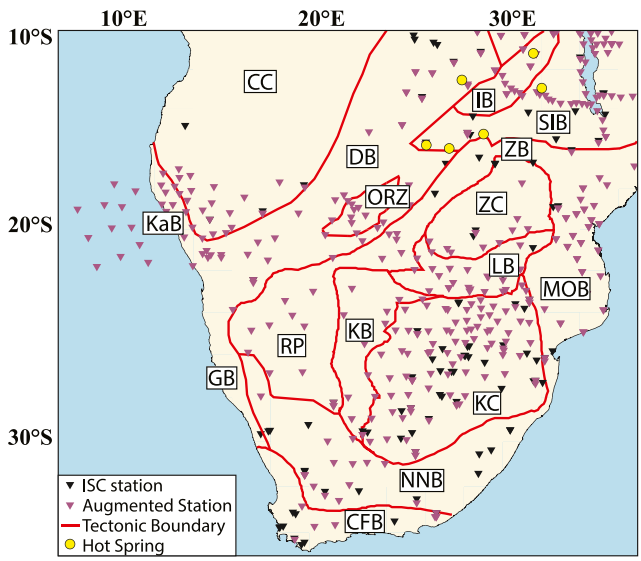

Figure 1. Map of southern Africa showing the locations of seismic stations and the boundaries of tectonic provinces. Black triangles denote stations that are part of the global International Seismological Center catalog, and purple triangles denoted augmented stations. Yellow circles denote the locations of hot springs in Zambia. CC: Congo Craton, IB: Irumide Belt, SIB: Southern Irumide Belt, KaB: Kaoko Belt, DB: Damara Belt, ORZ: Okavango Rift Zone, ZB: Zambezi Belt, ZC: Zimbabwe Craton, LB: Limpopo Belt, MOB: Mozambique Orogenic Belt, GB: Gariep Belt, RP: Rehoboth Province, KB: Kheis Belt, KC: Kaapvaal Craton, NNB: Namaqua-Natal Belt, CFB: Cape Fold Belt. Tectonic boundaries are from Begg et al. (2009).

The Damara and Ghanzi-Chobe Belts (collectively referred to in this paper as the Damara Belt) separate the Congo Craton to the north from the Kalahari Craton to the south (Figure 1). Along the western coast of Africa, the Damara Belt converges with the Kaoko and Gariep Belts in western Namibia (Figure 1; Begg et al., 2009; Miller, 2008; Passchier et al., 2016). Since the area does not readily display many of the characteristics typical of a continental suture (e.g., Lehmann et al., 2016), early studies (Martin & Porada, 1977; Porada, 1979) attributed the Neoproterozoic Damara, Kaoko, and Gariep belts to a rift-rift-rift triple junction, situated atop a vertical mantle plume, that formed at about 1,000 Ma. These studies also suggested the Damara Belt later experienced a collisional deformation event, and they characterized the region as a compound orogen/aulacogen. However, later studies (e.g., Barnes & Sawyer, 1980; Kukla & Stanistreet, 1991) challenged the aulacogen hypothesis and instead explained the Damara Belt as resulting from subduction followed by collision. Paleomagnetic (Z. X. Li, Bogdanova, et al., 2008), isotopic (Foster et al., 2015), and sedimentary data (Becker et al., 2006; Hoffman & Halverson, 2008) also suggest that the Damara Belt was formed by the convergence of the Congo and Kalahari Cratons at ~590 Ma, making it the youngest mobile belt in south-central Africa.

Much of the Damara Belt was not impacted by later tectonic events (Miller, 2008), and it is the only Pan-African terrane that has not been associated with volcanic activity over the last 30 Ma (Peyve, 2011; Priestley et al., 2008). However, during the Cenozoic, the Okavango Rift Zone (ORZ) developed in northern Botswana (Figure 1). Some researchers (e.g., Fadel et al., 2020; Leseane et al., 2015; Modisi et al., 2000; Ortiz et al., 2019; Yu, Gao, et al., 2015, Yu et al., 2017) have proposed that the ORZ marks the southwestern termination of the EARS: a complex network of continental rifts and volcanic centers that extends through Ethiopia and Kenya, with branches around either side of the Tanzania Craton (e.g., Ebinger et al., 2013; Ebinger & Sleep, 1998; Foster et al., 1997; Furman et al., 2006; Nyblade & Robinson, 1994; Pik et al., 1998). Incipient rifting in the ORZ may have initiated between about 120 and 40 ka (Modisi et al., 2000; Moore & Larkin, 2001). However, the extent of rifting in the ORZ and its potential connection to the EARS is still debated. Pastier et al. (2017), for instance, used geodetic data and seismicity to argue that no rifting is occurring in the Okavango region; instead, they suggest this area is experiencing differential movement between the Congo and Kalahari Cratons. Based on their magnetotelluric investigation, Khoza et al. (2013) suggested that the ORZ does not display the geologic characteristics, such as thinned lithosphere or conductive mantle, typically associated with continental rifting. Given this, they suggested that rifting in the ORZ is driven by surface processes and is not linked to the EARS.

Given its differences from other African mobile belts, the lithospheric and sublithospheric mantle structure beneath the Damara Belt and the ORZ have been investigated by a number of previous geophysical studies. Some prior investigations have suggested that the upper mantle beneath the Damara Belt and the ORZ is anomalous compared to surrounding regions. For example, Begg et al. (2009) combined global seismic tomography observations with mantle petrology data and suggested that the lithosphere beneath the Damara Belt displays lower-than-average shear-wave velocities (Vs) that are significantly different from the higher Vs observed beneath the Congo and Kalahari cratons. They attributed the Vs variations to changes in temperature and suggested that the northeastern segment of the Damara Belt has higher temperatures at 150 km depth compared to the southwestern segment. Based on local travel-time tomography, Yu et al. (2015b, 2017) also advocated for a slow anomaly beneath the ORZ region of the Damara Belt and suggested the anomaly is associated with decompression melting in the incipient rifting environment. Ortiz et al. (2019) examined P- and S-wave data recorded by stations in Botswana and South Africa and found similar results, also advocating for thermal perturbations in the Damara Belt lithosphere associated with rifting. While they did not evaluate the Damara Belt specifically, Emry et al. (2019) saw similar structure to that indicated by Yu et al. (2017) and Ortiz et al. (2019). Anomalous structure beneath the Damara region has also been suggested by studies employing magnetotelluric data. For example, Akinremi et al. (2022) imaged highly conductive materials beneath the ORZ and attributed them to ascending fluids or melt associated with continental rifting. If anomalously slow upper mantle structure is present beneath the Damara Belt and the ORZ, it could indicate that this region is influenced by the African LLVP, similar to what is thought to be occurring within the EARS.

Other geophysical studies have not found anomalous mantle structure beneath the Damara region. Priestley et al. (2008), for instance, modeled multimode surface wave data to examine the V_S beneath Africa, and they suggested that the Damara Belt is underlain by relatively thick lithosphere and a high velocity upper mantle. Using a combined regional and global surface- and S-wave data set, Celli et al. (2020) also developed a V_S model for Africa and similarly observed fast, thick lithosphere under the Damara Belt. White-Gaynor et al. (2020, 2021) developed both body and surface wave tomography models for southern Africa and suggested the lithosphere beneath the Damara Belt is ∼130 km thick, much thinner than that beneath the adjacent Kalahari Craton (∼200 km). Velocity variations in their models at sublithospheric depths were attributed to lithospheric thickness differences as opposed to thermal perturbations in the upper mantle. Afonso et al. (2022) combined both land-based seismic and satellite gravity data to evaluate the thermochemical structure of central-southern Africa, and they also advocate for lithospheric thinning beneath the Damara Belt, without evidence for thermally perturbed upper mantle. Additionally, the Rayleigh wave tomography model from Pandey et al. (2022) shows fast seismic velocities beneath both the Congo and Kalahari Cratons as well as beneath the Damara region; however, this study argued that the lithosphere beneath the Damara Belt may be up to 200 km thick.

P-wave receiver functions have also been used to evaluate the mantle structure beneath south-central Africa, which is potentially relevant to the discrepancies in upper mantle structure beneath the Damara Belt and surrounding regions, as reviewed above. Most receiver function analyses indicate normal mantle transition zone (MTZ) thickness beneath much of the region (Blum & Shen, 2004; Boyce & Cottaar, 2021; Julià & Nyblade, 2013; Sun et al., 2018; Yu et al., 2020), thereby indicating that there are no thermal anomalies extending

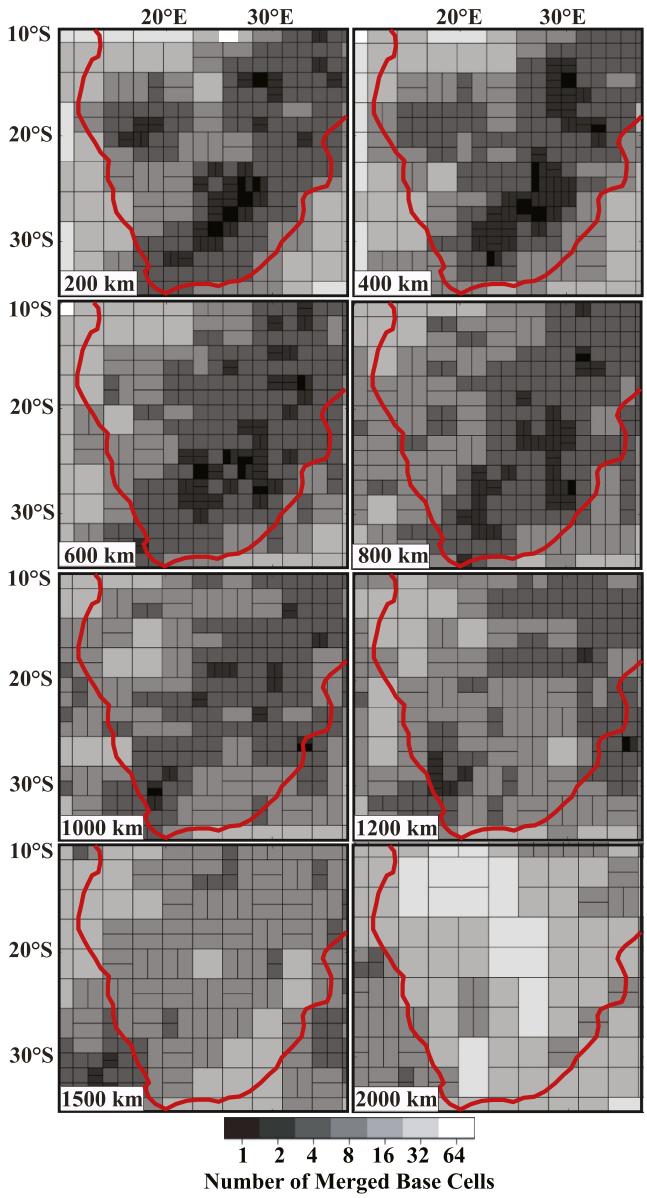

Figure 2. Adaptive grid cells from our tomographic model across southern Africa, shown at selected depths. Shading indicates the number of base cells (0.7° × 0.7°) included in each final cell. Darker shading indicates smaller cells, and lighter shading indicates larger cells. As explained in Section 3, the threshold for each cell is 900 ray paths; therefore, darker (smaller) cells highlight areas with greater ray path coverage and higher resolution.

across the MTZ. Sun et al. (2018), for example, suggested that any anomalously slow structure associated with the African LLVP has limited impact on the mid- and upper mantle beneath this region.

The lack of consensus regarding the mantle structure beneath south-central Africa stems from limited seismic network coverage in this region and from resolution gaps between local, regional, and global-scale investigations. Our model incorporates all available seismic data collected across Africa, and our adaptively parameterized tomography approach helps to bridge some of these resolution gaps (Hansen et al., 2012; Hansen & Nyblade, 2013; Saeidi et al., 2023). Collectively this allows us to better image the mantle structure beneath the Damara Belt and surrounding areas and to evaluate how that structure may influence tectonic features observed at the surface.

3. Data and Methodology

We have compiled a comprehensive data set of P-wave travel-time residuals to develop a new high-resolution model of the African mantle structure. Much of our data have been acquired from a recent version of the International Seismological Center (ISC) catalog, which includes travel-time residuals from about 562,000 earthquakes that occurred between 1964 and 2016 (Engdahl et al., 1998; Weston et al., 2018). A range of P-wave phases (P, Pg, Pn, pP, and PKP) are employed to provide broad sampling of the Earth's interior structure, and the global ISC catalog contains about 30 million travel-time residuals. However, to further increase the resolution of our model beneath Africa, data from 60 additional seismic networks (1,576 stations) that are not included in the ISC catalog were used to augment the global data set. The augmented data set is similar to that used by Saeidi et al. (2023); however, we now also include data from earthquakes with moment magnitudes (M_w) > 5.5 recorded by the SAFARI (XK) network, which operated from 2012 to 2014 (Gao et al., 2012). Since this network was deployed in close vicinity to the Damara Belt, it provides critical data for our study. The magnitude and epicentral distance criteria (30°–90°) imposed on the selected teleseismic events help to ensure high signal-to-noise ratio P-wave arrivals. Vertical component seismograms were examined using an iterative, weighted stacking and cross-correlation scheme (Hansen et al., 2020; Pavlis & Vernon, 2010; Saeidi et al., 2023) to robustly pick P-wave onsets, and similar to the ISC catalog, travel-time residuals were computed relative to the AK135 global velocity model (Kennett et al., 1995). The augmented data set employed in this study includes a total of 109,641 P-wave travel-time residuals from stations across Africa (Figure 1).

Both the global ISC and the augmented African data sets were used to develop an adaptive model parameterization for our tomographic inversion. That is, the model gridding is adapted to variations in the ray path coverage, which prevents regions with poor coverage from becoming over-parameterized and those with dense coverage from losing resolution due to averaging (Hansen et al., 2012; Kárason & van der Hilst, 2000; C. Li, Bogdanova, et al., 2008; Saeidi et al., 2023). The smallest grid cells in our model are 0.7° × 0.7°; however, if a cell does not contain at least 900 ray paths, it is merged with neighboring cells until the ray count threshold is met. Our current model contains 764,406 adaptive grid cells, examples of which are shown in Figure 2.

Together, the adaptive grid and the combined ISC-African travel-time residuals are inverted using an iterative damped least square approach (Paige & Saunders, 1982). The higher quality African data are given twice the weight in the inversion in order to balance this data set against the larger but somewhat noisier ISC catalog. Additionally, since the small incidence angle of P-waves can cause crustal anomalies to "smear" into deeper

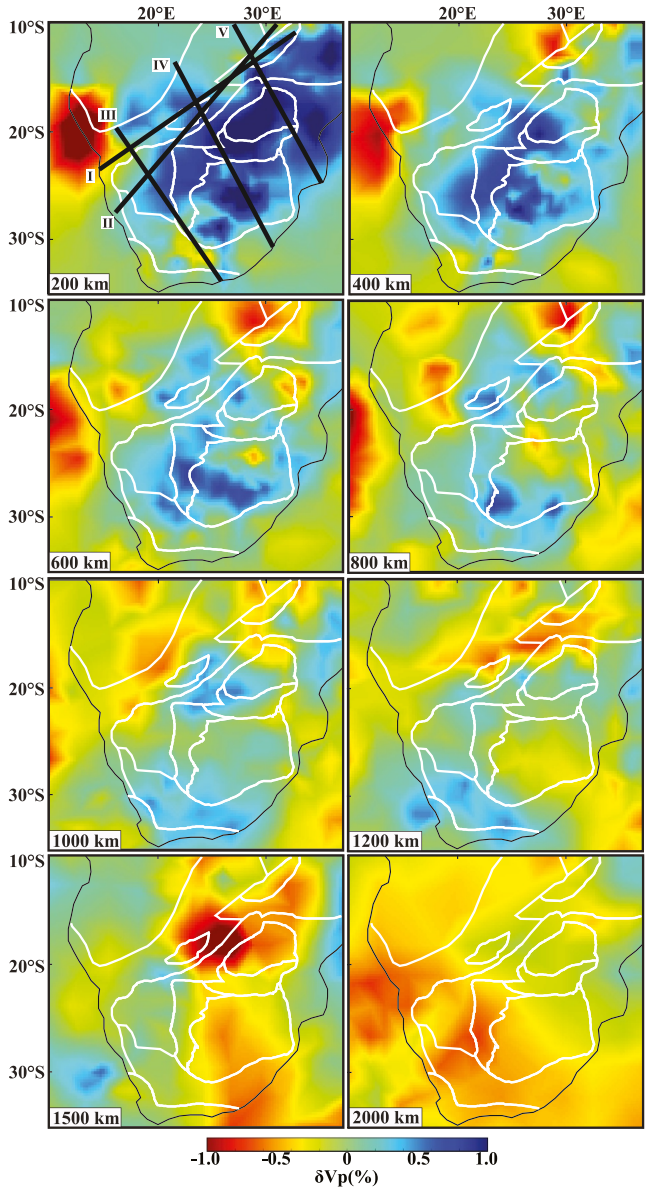

Figure 3. Map-view images of our tomographic model across southern Africa, showing P-wave velocity perturbations from the AK135 reference model (δV_P; Kennett et al., 1995) at selected depths. White lines show the same tectonic boundaries as in Figure 1. Black lines labeled I to V on the 200 km panel show the locations of the cross-sectional profiles in Figure 4.

portions of the model space, we incorporate the 3-D CRUST1.0 model (Laske et al., 2012) into our inversion to balance the crustal and upper mantle contributions to the misfit (C. Li et al., 2006, 2008). Kárason (2002) and C. Li, Bogdanova, et al. (2008) provide a detailed description of the sensitivity matrix calculations, where the employed approach allows low-frequency data to constrain long-wavelength structures without preventing short-period data from resolving small-scale features.

The global inversion accounts for structural heterogeneities outside the study region, but as noted above, we are interested in the mantle structure beneath the Damara Belt. Figure 3 shows our P-wave velocity perturbations, relative to the AK135 reference model (Kennett et al., 1995), at select upper mantle depths, with corresponding cross-sections shown in Figure 4. These results were obtained after 200 iterations of the inversion and correspond to a 93% reduction in the error function. The length of the residual vector decreased from 0.95 to 0.25 s, indicating the improved data fit between the starting and the final models. For comparison, the tomographic results obtained using only the ISC travel-time data set (i.e., excluding the augmented data) are shown in Supporting Information S1, Figure S1. As illustrated, the augmented data set significantly improves model recovery across the continent.

4. Results and Resolution Tests

Comparing our tomographic results to other global (Hosseini, 2016; C. Li, Bogdanova, et al., 2008; Lu et al., 2019; Montelli et al., 2004; Simmons et al., 2012) as well as continental- and regional-scale (Adams & Nyblade, 2011; Begg et al., 2009; Boyce et al., 2021; Fishwick, 2010; Hansen et al., 2012; Priestley et al., 2008) models, we observe several major anomalies that are broadly consistent across all studies. First, slow seismic velocities are seen beneath much of eastern Africa, and this reflects the anomalous structure of the EARS. Second, a large seismically slow anomaly is present in the lower mantle beneath southern Africa, starting above the CMB and extending upwards to the northeast. As noted in Section 1, this feature is interpreted to reflect the African LLVP. Third, fast seismic velocities in our model are seen in both central-western and southern Africa, and these are associated with the Congo and Kalahari Cratons, respectively (Figures 3 and 4).

In the Damara Belt region, we observe slow mantle velocities, but they are constrained to depths greater than ~1,200 km. As illustrated in Profiles I–IV (Figure 4), this is the case beneath both the ORZ and the rest of the Damara Belt. The P-wave velocity perturbation associated with this slow structure averages about −1%, though it reaches about −1.5% at its peak. That said, Profiles I, II, and V (Figure 4) show that the slow velocities ascend to shallower depths on the northeast side of the study region, crossing the MTZ near the Irumide Belt, and reaching the upper mantle beneath the EARS. Our results also suggest a change in the fast upper mantle seismic velocities from southwest to northeast. Beneath the Damara Belt, fast anomalies extend to ~400–500 km depth (depending on the profile), but beneath the Irumide Belt, the fast velocities are constrained to the upper ~200–300 km of the mantle.

Several types of resolution tests have been performed to evaluate our model. First, checkerboard resolution tests, which are widely employed for tomographic assessment, were generated. The input checkers were 5° × 5°, with thicknesses of 35 km and with ±2% P-wave velocity perturbations. These synthetic anomalies were centered at different depths within the model space to assess both lateral and vertical resolution. It is important to note that the checkers were projected onto our adaptive grid (Figure 2), which can sometimes lead to small distortions in their shape and/or thickness. Synthetic travel-times were generated and inverted using the same parameters as those

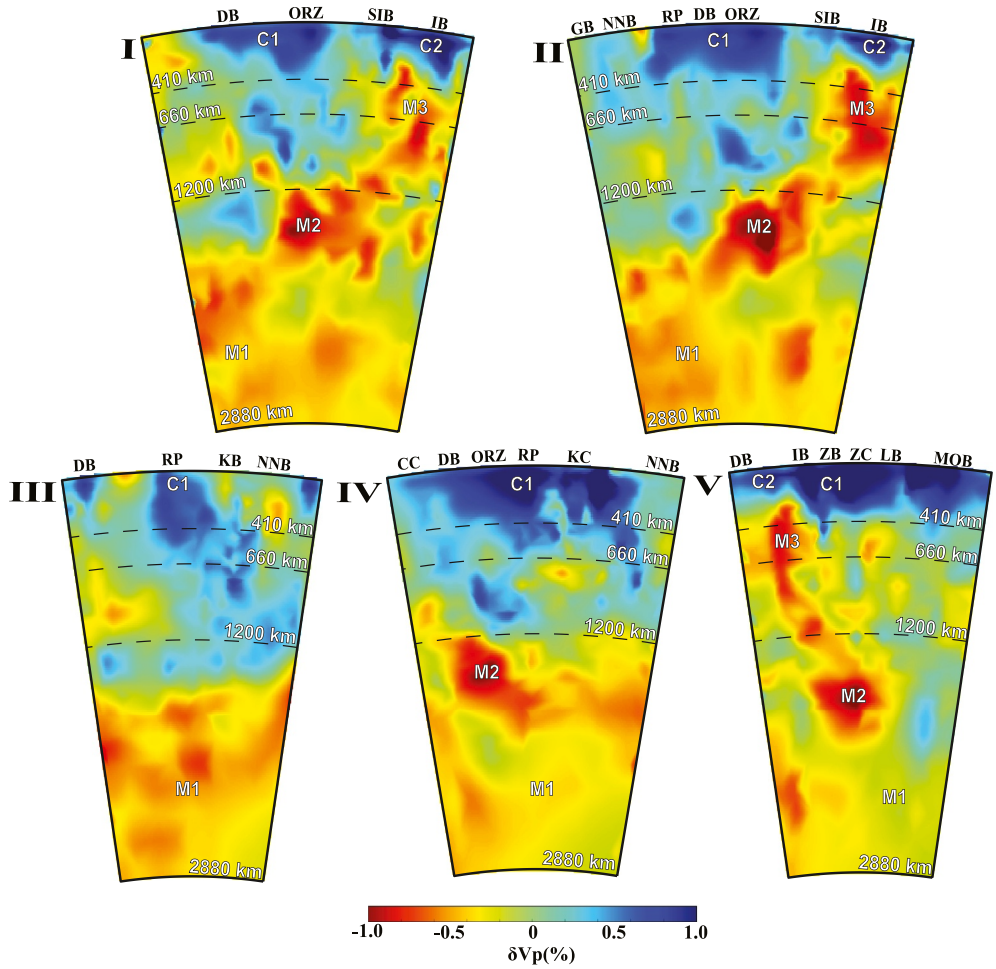

Figure 4. Cross-sectional profiles across the study region (locations are shown in Figure 3). Select depths and features discussed in the text are labeled. Abbreviations for tectonic features are the same as in Figure 1. We note that Profiles I and II are the same as those from White-Gaynor et al. (2020), though our model is plotted to deeper depth.

used for the real data, but noise was added to the synthetic travel-times as a Gaussian residual time error with a standard deviation of 0.25 s, which corresponds to the weighted average of the residual remaining in our model after inversion. This approach reproduces the fit to the synthetic data as that obtained in our actual model (Hansen et al., 2014; Rawlinson et al., 2014). Figure 5 shows examples of the recovered checkerboard tests at different depths, with additional examples shown in Supporting Information S1, Figures S2 and S3. Amplitude recovery varies with depth, and the best recovery (more than 60%) is obtained between about 600 and 1,000 km. At lithospheric depths (~100–200 km), particularly in the northwestern part of the study region under the Congo Craton, amplitude recovery reduces to ~30%. This is largely due to the lack of seismic station coverage in that area (Figure 1). Similarly, given the smaller number of seismic phases that traverse the deep mantle, amplitude recovery below about 1,500 km depth is reduced. The checkerboard pattern is generally well recovered, illustrating the high resolution and reliability of our model, especially when compared to the size of the investigated features (Figures 3 and 4). These tests also provide information on the amount of vertical smearing in our model, caused by the steep incidence angle of P-wave arrivals (Section 3). In the upper mantle (above ~400 km depth), ~200–250 km of vertical smearing is observed (Figure S3 in Supporting Information S1); however, at deeper depths, the degree of vertical smearing is reduced to ~100 km.

We also designed a series of targeted resolution tests to evaluate features of interest in our tomographic results (Figures 3 and 4). Various synthetic anomalies were incorporated into a single input model and were varied to match the observed velocity features as close as possible. Our first test (Figure 6) included two fast anomalies (2.5% and 1.5%, respectively) with thicknesses of 250 and 100 km to match the fast seismic structure beneath the

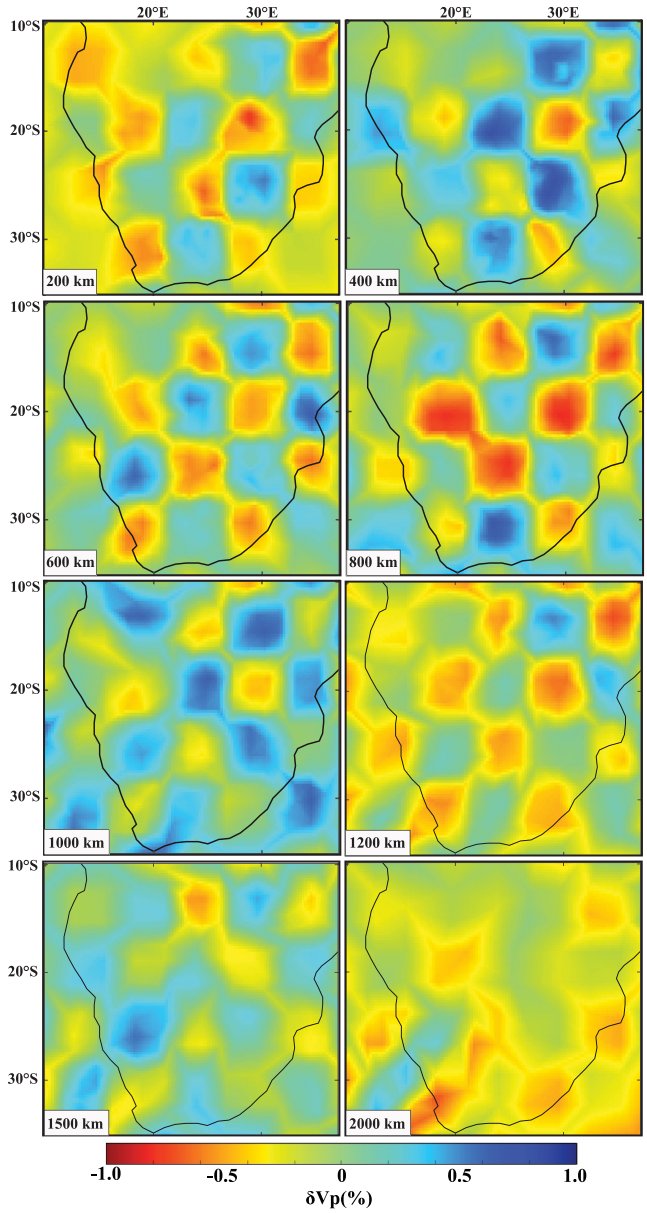

Figure 5. Checkerboard resolution tests at selected mantle depths. All models were generated with 5° × 5° input checkers that had ±2% P-wave velocity perturbations (δV_P) compared to the reference model (Kennett et al., 1995).

Damara Belt and the Irumide Belt (anomalies C1 and C2, Figure 4), respectively. The resolution test also included a slow anomaly (−0.7%) below ∼1,600 km depth, corresponding to the African LLVP above the CMB (anomaly M1, Figure 4). A second, more pronounced slow anomaly (−1.4%) below ∼1,200 km was also included to match our model (anomaly M2, Figure 4). Similar to the checkerboard tests, the targeted anomalies have been projected onto the adaptive grid (Figure 2), and the inversion was run with synthetic travel-times that had the same Gaussian noise application. We then ran two additional targeted resolution tests that included the same synthetic anomalies described above, but we also introduced a stair-step pattern to mimic the rise of the slow structure to shallower depths at the northeastern part of the study area (anomaly M3, Figure 4). These additional slow anomalies are 1% slower than the reference model, and we examined cases where the slow structure ascended to 660 km depth (Figure S4 in Supporting Information S1) as well as to 300 km depth (Figure 7). While the results are impacted by some vertical smearing, this effect is fairly minimal. Of the different examined structures, only the third targeted resolution test, which allows the slow anomalies to cross the MTZ and extend into the upper mantle near the EARS (Figure 7), closely approximates the actual model (Figure 4).

5. Discussion

The different resolution tests described in Section 4 (Figures 5–7; Figures S2–S4 in Supporting Information S1) demonstrate that the P-wave velocity structure highlighted in Figures 3 and 4 is robust. This is further illustrated by the extensive ray path coverage (Figures S5–S7 in Supporting Information S1) as well as by the dense adaptive gridding (Figure 2) in our model space across the Damara Belt and the surrounding, examined regions. At shallow depths, the Damara Belt is characterized by seismic velocities that are about 2.5% faster than the reference model (Kennett et al., 1995). Considering the level of vertical smearing indicated by our resolution tests (Figure S3 in Supporting Information S1) as well as how the synthetic anomalies project onto the adaptive grid, we estimate the lithosphere in this region is 150–200 km thick, consistent with prior studies (e.g., Celli et al., 2020; Pandey et al., 2022; Priestley et al., 2008; White-Gaynor et al., 2020, 2021). Further, slow anomalies beneath the Damara Belt and the ORZ in our model are constrained to the lower mantle (below ∼1,200 km depth; Figures 3 and 4). These findings agree with the studies discussed in Section 2 that argue for unperturbed upper mantle beneath the Damara region (Afonso et al., 2022; Celli et al., 2020; Pandey et al., 2022; Priestley et al., 2008; White-Gaynor et al., 2020, 2021).

To the northeast, the lithosphere beneath the Irumide Belt and the EARS appears to be somewhat thinner than that beneath the Damara Belt region (Figure 4). Again, taking the level of vertical smearing indicated by our resolution tests into account (Figures 5–7; Figures S2–S4 in Supporting Information S1), we approximate the lithosphere in this area to be ∼100 km thick. This agrees fairly well with the ∼100–150 km thickness estimated by previous studies (e.g., Adams et al., 2018; O'Donnell et al., 2013; Sarafian et al., 2018). Additionally, the slow structure seen at depth beneath the Damara Belt ascends toward the northeast portion of the study area, crossing the MTZ beneath the Irumide Belt and entering the upper mantle beneath the EARS (Figure 4). It is worth noting that these observations agree with some prior global tomography models (e.g., Burdick et al., 2017; Hosseini, 2016; Houser et al., 2008; Koelemeijer et al., 2016; Lu et al., 2019; Simmons et al., 2010, 2012; Tesoniero et al., 2015), which illustrate similar velocity patterns but with lower resolution (see Figures S8–S13 in Supporting Information S1). Our cross-sectional profiles I and II (Figure 4) are the same as those in the regional study by White-Gaynor et al. (2020), who also found slow seismic velocities beneath the northeastern ends of Profiles I and II, though their models are limited to the upper 900 km of the mantle.

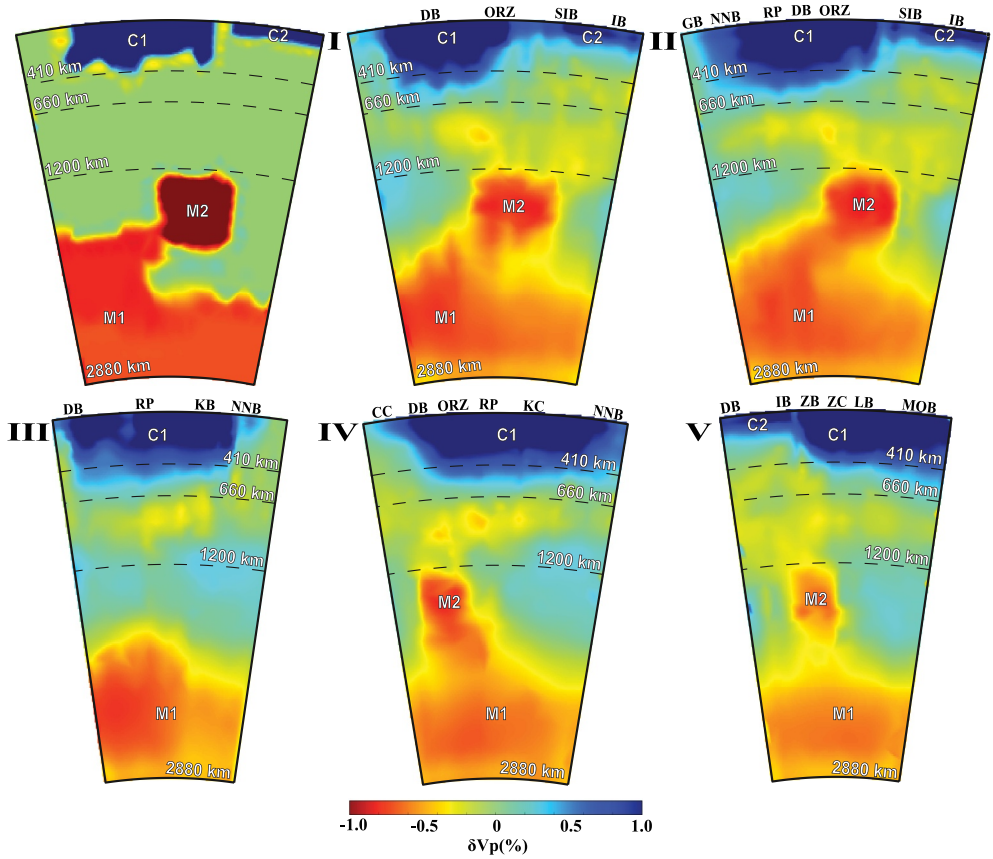

Figure 6. Targeted resolution test. The input model along Profile II is shown in the top left panel. Fast anomalies C1 and C2 represent the cratonic lithosphere under the Damara region and beneath the Irumide Belt, respectively. Slow anomaly M1 represents the African Large Low Velocity Province in the deep mantle, extending upwards from the core-mantle boundary to ~1,600 km depth. Slow anomaly M2 represents the slow structure seen in our model (Figure 4) just below 1,200 km depth. Other panels show the recovered results along all five cross-sectional profiles (I-V, Figure 4). Abbreviations for tectonic features are the same as in Figure 1.

The anomalously slow southwest-to-northeast velocity structure we observe along the Damara Belt and into eastern Africa (Figure 4) is best attributed to the African LLVP rising from the CMB. Beneath the Damara Belt region, the LLVP is constrained to depths greater than ~1,200 km (Figure 4). This is consistent with prior receiver function investigations that indicate normal MTZ thickness beneath the study area (Blum & Shen, 2004; Boyce & Cottaar, 2021; Julià & Nyblade, 2013; Sun et al., 2018; Yu et al., 2020), and collectively, the results suggest that the LLVP has little influence on the mid- or upper mantle structure beneath the Damara Belt. Therefore, if the LLVP does extend to the north or northwest beneath south-central Africa, it does so within the lower mantle. That said, beneath the Irumide Belt and the EARS, the mantle structure is quite different. Yuan & Li (2022) suggested that the African LLVP reaches 1,500 km above the CMB, but our results and others (Bastow et al., 2008; Grijalva et al., 2018; Halldórsson et al., 2014; Hansen & Nyblade, 2013; Rajaonarison et al., 2023) indicate that this feature likely rises much higher, entering the upper mantle beneath the northeastern portion of our study area. These findings are also consistent with the receiver function results from Owens et al. (2000), Huerta et al. (2009), and Mulibo and Nyblade (2013), which all suggest a perturbed MTZ beneath this area, consistent with a thermal anomaly that likely crosses from the lower to the upper mantle. It is also worth noting that the fast velocities bordering the upper edge of the LLVP anomaly between ~700 and 1,300 km depth (Profiles I–II, Figure 4) may result from an abrupt change in mantle characteristics, consistent with the concept that the LLVP has sharp, defined boundaries indicative of a thermochemical origin (e.g., Ni et al., 2002; To et al., 2005).

The trend of the LLVP and the velocity structure we have imaged also correlate well with various surface observations. For example, the northeastern portion of the study area, where the LLVP crosses into the upper mantle, displays significant geothermal activity, as evident by the many hot springs in this region (Figure 1). This may

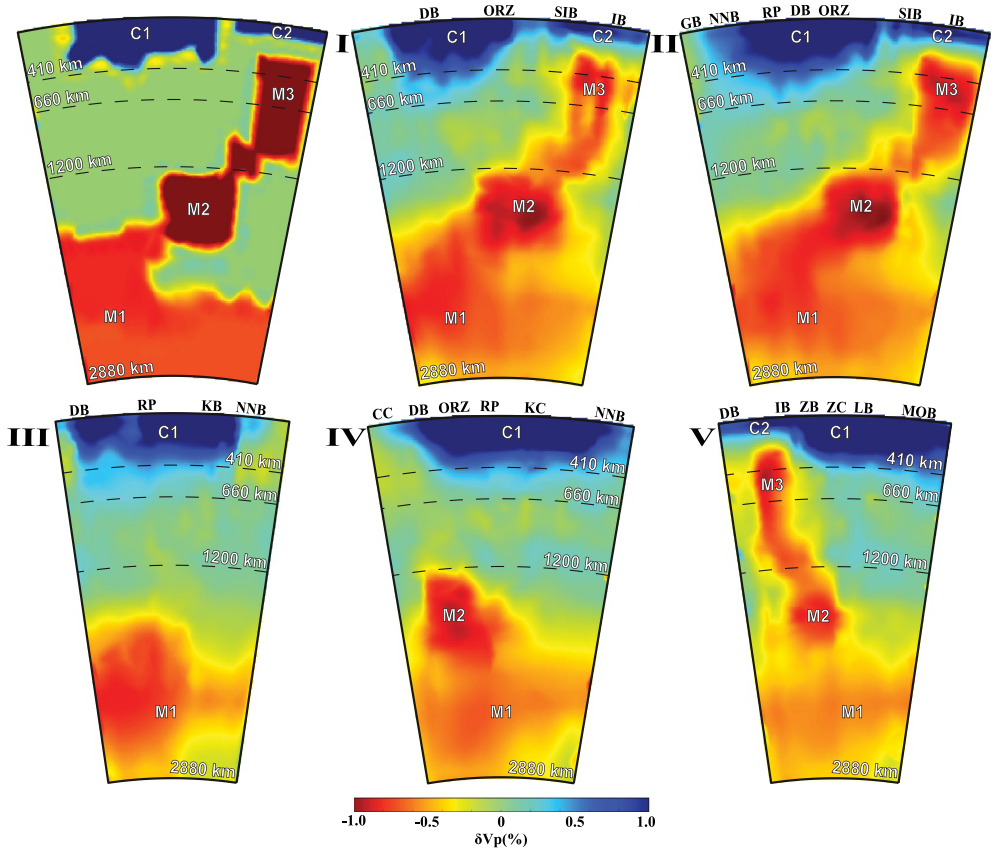

Figure 7. Same as Figure 6, but now the input model (top left panel) includes an additional slow anomaly, M3, that extends across the transition zone and into the upper mantle beneath the northeastern part of our study area.

suggest that this area is associated with elevated heat flow (e.g., Elbarbary et al., 2022; Macgregor, 2020), though we note that direct measurements (Ballard et al., 1987; Ballard & Pollack, 1987; Nyblade et al., 1990) do not find significant heat flow variations across this portion of south-central Africa. However, to the southwest, where the LLVP is constrained to the deeper mantle, no such geothermal features are observed. As mentioned in Section 2, the Damara Belt has not experienced any volcanic activity over the last 30 Ma (Peyve, 2011; Priestley et al., 2008) and this could be due to the deep-seated (LLVP) volcanic source (Profiles III–IV, Figure 4). Additionally, studies of dynamic topography across Africa show consistency with our tomographic results. For example, Lithgow-Bertelloni and Silver (1998), Gurnis et al. (2000), and Artemieva and Vinnik (2016) evaluated the source of elevated topography across southern Africa and concluded that a low-density, high-temperature mantle upwelling at sublithospheric depths must contribute to surface uplift. Globig et al. (2016) and Gedamu et al. (2021) examined the Afar region in eastern Africa and suggested that sublithospheric mantle flow and buoyancy provide a dynamic contribution to the surface elevation and deformation patterns in that area. These observations are consistent with the LLVP trend interpreted from our model. Further, the shallow portion of the LLVP may significantly influence the complex continental rift pattern seen throughout eastern Africa (Bastow et al., 2008; French & Romanowicz, 2015; Hansen et al., 2012); however, such rifting activity is not observed throughout most of the Damara Belt. The nature of rifting occurring in the ORZ is still a matter of debate (e.g., Pastier et al., 2017), but if the rifting is associated with the southwestern termination of the EARS, as suggested by some prior studies (Akinremi et al., 2022; Begg et al., 2009; Ortiz et al., 2019; Yu, Gao, et al., 2015, 2017), then it must be influenced by extensional processes driven by something other than the LLVP (e.g., Khoza et al., 2013).

6. Conclusion

Our new adaptively parameterized teleseismic P-wave tomography model provides further insights on the geodynamic structure beneath the Damara Belt and its surrounding regions. Our findings challenge the notion that the

Damara Belt and ORZ are underlain by a thermally perturbed, seismically slow upper mantle. Rather, we advocate that anomalously slow structure beneath this area is constrained to lower mantle depths of ∼1,200 km or greater. This suggests that the African LLVP does not extend into the upper mantle beneath south-central Africa. However, the slow structure at depth beneath the Damara Belt obliquely rises toward the northeast, crossing the MTZ near the Irumide Belt, and extending into the upper mantle beneath the EARS. This variable slow structure is best attributed to the southwest-to-northeast rise of the African LLVP, and its trend correlates with surface tectonic observations, including variations in heat flow, the distribution of geothermal features, the locations of rifts, and estimates of dynamic topography.

Data Availability Statement

The Augmented African Data set integrates seismic data from temporary and national seismograph networks identified by their respective codes (Albuquerque Seismological Laboratory (ASL)/USGS, 1993; Albuquerque Seismological Laboratory/USGS, 2014; Botswana Geoscience Institute, 2001; Centre for Geodesy & Geodynamics, 2009; Deschamps Anne et al., 2007; Ebinger, 2007, 2012, 2013, 2014, 2018; Gaherty et al., 2013; Gaherty & Shillington, 2010; Gao, 2009; Gao et al., 2012; GEOFON Data Centre, 1993; Ghana Geological Survey, 2012; Hammond et al., 2011; Heit et al., 2010; Helffrich & Fonseca, 2011; Institute Earth Sciences "Jaume Almera" CSIC (ICTJA Spain), 2007; Keir et al., 2016; Keir & Hammond, 2009; Keranen, 2013; Kind, 1998; Leroy, 2003; Levander et al., 2009; Levèque, 2010; MedNet Project Partner Institutions, 1990; Nyblade, 2000, 2007, 2010, 2015a, 2015b, 2017; Owens & Nyblade, 1994; Penn State University, 2004; Roult et al., 2010; San Fernando Royal Naval Observatory (ROA) et al., 1996; Scripps Institution of Oceanography, 1986; Silver, 1997; Thomas, 2010; Tilmann et al., 2012; Utrecht University (UU Netherlands), 1983; Velasco et al., 2011; Vergne et al., 2014; Wiens & Nyblade, 2005; Wookey et al., 2011; Wysession et al., 2011). The facilities of SAGE Data Services, and specifically the SAGE Data Management Center, were used for access to waveforms and related metadata (http://ds.iris.edu/mda/). SAGE Data Services are funded through the Seismological Facilities for the Advancement of Geoscience (SAGE) Award of the National Science Foundation under Cooperative Support Agreement EAR-1851048. Some of the data visualizations were generated with Generic Mapping Tools (Wessel et al., 2013).

Acknowledgments
We thank JC Afonso and an anonymous reviewer for their thorough critiques of our manuscript. Some of the seismic data used in this study were collected by projects supported by the National Science Foundation (Grant 0440032, 0530062, 0824781, 1128936, and 1634108).

References

Adams, A., Miller, J., & Accardo, N. (2018). Relationships between lithospheric structures and rifting in the East African Rift System: A Rayleigh wave tomography study. *Geochemistry, Geophysics, Geosystems*, *19*(10), 3793–3810. https://doi.org/10.1029/2018GC007750

Adams, A., & Nyblade, A. (2011). Shear wave velocity structure of the southern African upper mantle with implications for the uplift of southern Africa. *Geophysical Journal International*, *186*(2), 808–824. https://doi.org/10.1111/j.1365-246X.2011.05072.x

Afonso, J. C., Ben-Mansour, W., O'Reilly, S. Y., Griffin, W. L., Salajeghegh, F., Foley, S., et al. (2022). Thermochemical structure and evolution of cratonic lithosphere in central and southern Africa. *Nature Geoscience*, *15*(5), 405–410. https://doi.org/10.1038/s41561-022-00929-y

Akinremi, S., Fadel, I., & van der Meijde, M. (2022). Crustal and upper mantle imaging of Botswana using magnetotelluric method. *Frontiers in Earth Science*, *10*. https://doi.org/10.3389/feart.2022.840703

Albuquerque Seismological Laboratory (ASL)/USGS. (1993). Global telemetered seismograph network (USAF/USGS) [Dataset]. International Federation of Digital Seismograph Networks. https://doi.org/10.7914/SN/GT

Albuquerque Seismological Laboratory/USGS. (2014). Global seismograph network (GSN - IRIS/USGS) [Dataset]. International Federation of Digital Seismograph Networks. https://doi.org/10.7914/SN/IU

Artemieva, I. M., & Vinnik, L. P. (2016). Density structure of the cratonic mantle in southern Africa: 1. Implications for dynamic topography. *Gondwana Research*, *39*, 204–216. https://doi.org/10.1016/j.gr.2016.03.002

Ballard, S., & Pollack, H. N. (1987). Diversion of heat by Archean cratons: A model for southern Africa. *Earth and Planetary Science Letters*, *85*(1–3), 253–264. https://doi.org/10.1016/0012-821X(87)90036-7

Ballard, S., Pollack, H. N., & Skinner, N. J. (1987). Terrestrial heat flow in Botswana and Namibia. *Journal of Geophysical Research*, *92*(B7), 6291–6300. https://doi.org/10.1029/JB092iB07p06291

Barnes, S.-J., & Sawyer, E. W. (1980). An alternative model for the Damara mobile belt: Ocean crust subduction and continental convergence. *Precambrian Research*, *13*(4), 297–336. https://doi.org/10.1016/0301-9268(80)90048-0

Bastow, I. D., Nyblade, A. A., Stuart, G. W., Rooney, T. O., & Benoit, M. H. (2008). Upper mantle seismic structure beneath the Ethiopian hot spot: Rifting at the edge of the African low-velocity anomaly. *Geochemistry, Geophysics, Geosystems*, *9*(12). https://doi.org/10.1029/2008GC002107

Becker, T., Schreiber, U., Kampunzu, A. B., & Armstrong, R. (2006). Mesoproterozoic rocks of Namibia and their plate tectonic setting. *Journal of African Earth Sciences*, *46*(1–2), 112–140. https://doi.org/10.1016/j.jafrearsci.2006.01.015

Begg, G. C., Griffin, W. L., Natapov, L. M., O'Reilly, S. Y., Grand, S. P., O'Neill, C. J., et al. (2009). The lithospheric architecture of Africa: Seismic tomography, mantle petrology, and tectonic evolution. *Geosphere*, *5*(1), 23–50. https://doi.org/10.1130/GES00179.1

Benoit, M. H., Nyblade, A. A., Owens, T. J., & Stuart, G. (2006). Mantle transition zone structure and upper mantle S velocity variations beneath Ethiopia: Evidence for a broad, deep-seated thermal anomaly. *Geochemistry, Geophysics, Geosystems*, *7*(11). https://doi.org/10.1029/2006GC001398

Benoit, M. H., Nyblade, A. A., & VanDecar, J. C. (2006). Upper mantle P-wave speed variations beneath Ethiopia and the origin of the Afar hotspot. *Geology*, *34*(5), 329–332. https://doi.org/10.1130/G22281.1

Blum, J., & Shen, Y. (2004). Thermal, hydrous, and mechanical states of the mantle transition zone beneath southern Africa. *Earth and Planetary Science Letters*, *217*(3–4), 367–378. https://doi.org/10.1016/S0012-821X(03)00628-9

Botswana Geoscience Institute. (2001). Botswana seismological network [Dataset]. International Federation of Digital Seismograph Networks. https://doi.org/10.7914/SN/BX

Boyce, A., Bastow, I. D., Cottaar, S., Kounoudis, R., Guilloud De Courbeville, J., Caunt, E., & Desai, S. (2021). AFRP20: New P -Wavespeed model for the African mantle reveals two whole-mantle plumes below East Africa and neoproterozoic modification of the Tanzania Craton. *Geochemistry, Geophysics, Geosystems*, *22*(3). https://doi.org/10.1029/2020GC009302

Boyce, A., & Cottaar, S. (2021). Insights into deep mantle thermochemical contributions to African magmatism from converted seismic phases. *Geochemistry, Geophysics, Geosystems*, *22*(3), 1–25. https://doi.org/10.1029/2020GC009478

Burdick, S., Vernon, F. L., Martynov, V., Eakins, J., Cox, T., Tytell, J., et al. (2017). Model update May 2016: Upper-mantle heterogeneity beneath north America from travel-time tomography with global and USArray data. *Seismological Research Letters*, *88*(2A), 319–325. https://doi.org/10.1785/0220160186

Celli, N. L., Lebedev, S., Schaeffer, A. J., & Gaina, C. (2020). African cratonic lithosphere carved by mantle plumes. *Nature Communications*, *11*(1), 92. https://doi.org/10.1038/s41467-019-13871-2

Centre for Geodesy & Geodynamics. (2009). Nigerian National Network of Seismographi Stations (NNNSS) [Dataset]. International Federation of Digital Seismograph Networks. https://doi.org/10.7914/SN/NJ

Chang, S. J., Kendall, E., Davaille, A., & Ferreira, A. M. (2020). The evolution of mantle plumes in East Africa. *Journal of Geophysical Research: Solid Earth*, *125*(12). https://doi.org/10.1029/2020JB019929

Chorowicz, J. (2005). The East African rift system. *Journal of African Earth Sciences*, *43*(1–3), 379–410. https://doi.org/10.1016/j.jafrearsci.2005.07.019

Corti, G. (2009). Continental rift evolution: From rift initiation to incipient break-up in the Main Ethiopian Rift, East Africa. *Earth-Science Reviews*, *96*(1–2), 1–53. https://doi.org/10.1016/j.earscirev.2009.06.005

Deschamps, A., Déverchère, J., & Ferdinand, R. W. (2007). SEISMOTANZ'07 [Dataset]. RESIF - Réseau Sismologique et géodésique Français. https://doi.org/10.15778/RESIF.ZS2007

De Waele, B., Liégeois, J. P., Nemchin, A. A., & Tembo, F. (2006). Isotopic and geochemical evidence of Proterozoic episodic crustal reworking within the Irumide Belt of south-central Africa, the southern metacratonic boundary of an Archaean Bangweulu Craton. *Precambrian Research*, *148*(3–4), 225–256. https://doi.org/10.1016/j.precamres.2006.05.006

de Wit, M. J., de Ronde, C. E. J., Tredoux, M., Roering, C., Hart, R. J., Armstrong, R. A., et al. (1992). Formation of an Archaean continent. *Nature*, *357*(6379), 553–562. https://doi.org/10.1038/357553a0

Dziewonski, A. M., & Anderson, D. L. (1984). Seismic Tomography of the Earth's Interior: The first three-dimenstional models of the earth's structure promise to answer some basic questions of geodynamics and signify a revolution in earth science. *American Scientist*, *72*(5), 483–494. Retrieved from https://www.jstor.org/stable/27852863

Ebinger, C. (2007). AFAR07 [Dataset]. International Federation of Digital Seismograph Networks. https://doi.org/10.7914/SN/ZE_2007

Ebinger, C. (2012). Dynamics of the lake Kivu system [Dataset]. International Federation of Digital Seismograph Networks. https://doi.org/10.7914/SN/YA_2012

Ebinger, C. (2013). Magadi-natron magmatic rifting studies [Dataset]. International Federation of Digital Seismograph Networks. https://doi.org/10.7914/SN/XJ_2013

Ebinger, C. (2014). Southern Lake Tanganyika experiment [Dataset]. International Federation of Digital Seismograph Networks. https://doi.org/10.7914/SN/ZV_2014

Ebinger, C. (2018). Crust and mantle structure and the expression of extension in the Turkana Depression of Kenya and Ethiopia [Dataset]. International Federation of Digital Seismograph Networks. https://doi.org/10.7914/SN/Y1_2018

Ebinger, C. J., & Sleep, N. H. (1998). Cenozoic magmatism throughout east Africa resulting from impact of a single plume. *Nature*, *395*(6704), 788–791. https://doi.org/10.1038/27417

Ebinger, C. J., Van Wijk, J., & Keir, D. (2013). The time scales of continental rifting: Implications for global processes. *Special Papers - Geological Society of America*, *500*(11), 371–396. https://doi.org/10.1130/2013.2500(11

Elbarbary, S., Zaher, M. A., Saibi, H., Fowler, A.-R., & Saibi, K. (2022). Geothermal renewable energy prospects of the African continent using GIS. *Geothermal Energy*, *10*(8), 8. https://doi.org/10.1186/s40517-022-00219-1

Emry, E. L., Shen, Y., Nyblade, A. A., Flinders, A., & Bao, X. (2019). Upper mantle earth structure in Africa from full-wave ambient noise tomography. *Geochemistry, Geophysics, Geosystems*, *20*(1), 120–147. https://doi.org/10.1029/2018GC007804

Engdahl, E. R., van der Hilst, R., & Buland, R. (1998). Global teleseismic earthquake relocation with improved travel times and procedures for depth determination. *Bulletin of the Seismological Society of America*, *88*(3), 722–743. https://doi.org/10.1785/bssa0880030722

Fadel, I., Paulssen, H., van der Meijde, M., Kwadiba, M., Ntibinyane, O., Nyblade, A., & Durrheim, R. (2020). Crustal and upper mantle shear wave velocity structure of Botswana: The 3 April 2017 Central Botswana earthquake linked to the East African Rift System. *Geophysical Research Letters*, *47*(4). https://doi.org/10.1029/2019GL085598

Fishwick, S. (2010). Surface wave tomography: Imaging of the lithosphere-asthenosphere boundary beneath central and southern Africa? *Lithos*, *120*(1–2), 63–73. https://doi.org/10.1016/j.lithos.2010.05.011

Fonseca, J. F. B. D., Chamussa, J., Domingues, A., Helffrich, G., Antunes, E., van Aswegen, G., et al. (2014). MOZART: A seismological investigation of the East African rift in Central Mozambique. *Seismological Research Letters*, *85*(1), 108–116. https://doi.org/10.1785/0220130082

Foster, D. A., Ebinger, C. J., Mbede, E., & Rex, D. C. (1997). Tectonic development of the northern Taiizaiiian sector of the East African Rift System. *Journal of the Geological Society*, *154*(4), 689–700. https://doi.org/10.1144/gsjgs.154.4.0689

Foster, D. A., Goscombe, B. D., Newstead, B., Mapani, B., Mueller, P. A., Gregory, L. C., & Muvangua, E. (2015). U–Pb age and Lu–Hf isotopic data of detrital zircons from the Neoproterozoic Damara Sequence: Implications for Congo and Kalahari before Gondwana. *Gondwana Research*, *28*(1), 179–190. https://doi.org/10.1016/j.gr.2014.04.011

French, S. W., & Romanowicz, B. A. (2015). Broad plumes rooted at the base of the Earth's mantle beneath major hotspots. *Nature*, *525*(7567), 95–99. https://doi.org/10.1038/nature14876

Furman, T., Bryce, J., Rooney, T. O., Hanan, B., Yirgu, G., & Ayalew, D. (2006). Heads and tails: 30 million years of the Afar plume. *Geological Society, London, Special Publications*, *259*(1), 95–119. https://doi.org/10.1144/GSL.SP.2006.259.01.09

Gaherty, J., Ebinger, C. J., Nyblade, A. A., & Shillington, D. J. (2013). Study of extension and maGmatism in Malawi aNd Tanzania [Dataset]. International Federation of Digital Seismograph Networks. https://doi.org/10.7914/SN/YQ_2013

Gaherty, J., & Shillington, D. (2010). 2009 Malawi earthquake RAMP response [Dataset]. International Federation of Digital Seismograph Networks. https://doi.org/10.7914/SN/YI_2010

Gao, S. S. (2009). Afar depression dense seismic array [Dataset]. International Federation of Digital Seismograph Networks. https://doi.org/10.7914/SN/ZK_2009

Gao, S. S., Liu, K., Abdelsalam, M., & Hogan, J. (2012). Seismic arrays for African rift initiation [Dataset]. International Federation of Digital Seismograph Networks. https://doi.org/10.7914/SN/XK_2012

Gedamu, A. A., Eshagh, M., & Bedada, T. B. (2021). Effects of mantle dynamics on estimating effective elastic thickness of the lithosphere. *Journal of African Earth Sciences*, *183*, 104318. https://doi.org/10.1016/j.jafrearsci.2021.104318

GEOFON Data Centre. (1993). GEOFON seismic network [Dataset]. Deutsches GeoForschungsZentrum GFZ. https://doi.org/10.14470/TR560404

Ghana Geological Survey. (2012). Ghana digital seismic network [Dataset]. International Federation of Digital Seismograph Networks. https://doi.org/10.7914/SN/GH

Globig, J., Fernàndez, M., Torne, M., Vergés, J., Robert, A., & Faccenna, C. (2016). New insights into the crust and lithospheric mantle structure of Africa from elevation, geoid, and thermal analysis. *Journal of Geophysical Research: Solid Earth*, *121*(7), 5389–5424. https://doi.org/10.1002/2016JB012972

Grijalva, A., Nyblade, A. A., Homman, K., Accardo, N. J., Gaherty, J. B., Ebinger, C. J., et al. (2018). Seismic evidence for plume- and craton-influenced upper mantle structure beneath the northern Malawi rift and the Rungwe volcanic province, east Africa. *Geochemistry, Geophysics, Geosystems*, *19*(10), 3980–3994. https://doi.org/10.1029/2018GC007730

Gurnis, M., Mitrovica, J. X., Ritsema, J., & van Heijst, H.-J. (2000). Constraining mantle density structure using geological evidence of surface uplift rates: The case of the African superplume. *Geochemistry, Geophysics, Geosystems*, *1*(7). https://doi.org/10.1029/2005gc000928

Halldórsson, S. A., Hilton, D. R., Scarsi, P., Abebe, T., & Hopp, J. (2014). A common mantle plume source beneath the entire East African Rift System revealed by coupled helium-neon systematics. *Geophysical Research Letters*, *41*(7), 2304–2311. https://doi.org/10.1002/2014GL059424

Hammond, J., Goitom, B., Kendall, J. M., & Ogubazghi, G. (2011). Eritrea seismic project [Dataset]. International Federation of Digital Seismograph Networks. https://doi.org/10.7914/SN/5H_2011

Hansen, S. E., Carson, S. E., Garnero, E. J., Rost, S., & Yu, S. (2020). Investigating ultra-low velocity zones in the southern hemisphere using an Antarctic dataset. *Earth and Planetary Science Letters*, *536*, 116142. https://doi.org/10.1016/j.epsl.2020.116142

Hansen, S. E., Graw, J. H., Kenyon, L. M., Nyblade, A. A., Wiens, D. A., Aster, R. C., et al. (2014). Imaging the Antarctic mantle using adaptively parameterized P-wave tomography: Evidence for heterogeneous structure beneath West Antarctica. *Earth and Planetary Science Letters*, *408*, 66–78. https://doi.org/10.1016/j.epsl.2014.09.043

Hansen, S. E., & Nyblade, A. A. (2013). The deep seismic structure of the Ethiopia/Afar hotspot and the African superplume. *Geophysical Journal International*, *194*(1), 118–124. https://doi.org/10.1093/gji/ggt116

Hansen, S. E., Nyblade, A. A., & Benoit, M. H. (2012). Mantle structure beneath Africa and Arabia from adaptively parameterized P-wave tomography: Implications for the origin of Cenozoic Afro-Arabian tectonism. *Earth and Planetary Science Letters*, *319–320*, 23–34. https://doi.org/10.1016/j.epsl.2011.12.023

Heit, B., Yuan, X., Jokat, W., Weber, M., & Geissler, W. (2010). WALPASS network, Namibia, 2010/2012 [Dataset]. Deutsches GeoForschungsZentrum GFZ. https://doi.org/10.14470/1N134371

Helffrich, G., & Fonseca, J. (2011). Mozambique rift tomography [Dataset]. International Federation of Digital Seismograph Networks. https://doi.org/10.7914/SN/6H_2011

Hoffman, P., & Halverson, G. (2008). Otvi group of the western northern platform, the Eastern Kaoko Zone and the western Northern Margin Zone. In *The geology of Namibia* (pp. 69–136).

Hosseini, K. (2016). *Global multiple-frequency seismic tomography using teleseismic and core-diffracted body waves* (Dissertation). LMU.

Hosseini, K., Matthews, K. J., Sigloch, K., Shephard, G. E., Domeier, M., & Tsekhmistrenko, M. (2018). SubMachine: Web-based tools for exploring seismic tomography and other models of Earth's deep interior. *Geochemistry, Geophysics, Geosystems*, *19*(5), 1464–1483. https://doi.org/10.1029/2018GC007431

Hosseini, K., Sigloch, K., Tsekhmistrenko, M., Zaheri, A., Nissen-Meyer, T., & Igel, H. (2020). Global mantle structure from multifrequency tomography using P, PP and P-diffracted waves. *Geophysical Journal International*, *220*(1), 96–141. https://doi.org/10.1093/gji/ggz394

Houser, C., Masters, G., Shearer, P., & Laske, G. (2008). Shear and compressional velocity models of the mantle from cluster analysis of long-period waveforms. *Geophysical Journal International*, *174*(1), 195–212. https://doi.org/10.1111/j.1365-246X.2008.03763.x

Huerta, A. D., Nyblade, A. A., & Reusch, A. M. (2009). Mantle transition zone structure beneath Kenya and Tanzania: More evidence for a deep-seated thermal upwelling in the mantle. *Geophysical Journal International*, *177*(3), 1249–1255. https://doi.org/10.1111/j.1365-246X.2009.04092.x

Institute Earth Sciences "Jaume Almera" CSIC (ICTJA Spain). (2007). IberArray [Dataset]. International Federation of Digital Seismograph Networks. https://doi.org/10.7914/SN/IB

Johnson, S. P., Rivers, T., & De Waele, B. (2005). A review of the Mesoproterozoic to early Palaeozoic magmatic and tectonothermal history of south–central Africa: Implications for Rodinia and Gondwana. *Journal of the Geological Society*, *162*(3), 433–450. https://doi.org/10.1144/0016-764904-028

Julià, J., & Nyblade, A. A. (2013). Probing the upper mantle transition zone under Africa with P520s conversions: Implications for temperature and composition. *Earth and Planetary Science Letters*, *368*, 151–162. https://doi.org/10.1016/j.epsl.2013.02.021

Kárason, H. (2002). *Constraints on mantle convection from seismic tomography and flow modeling* (Doctoral dissertation). Massachusetts Institute of Technology.

Kárason, H., & van der Hilst, R. D. (2000). Constraints on mantle convection from seismic tomography. *Geophysical Monograph Series*, *121*, 257–276. https://doi.org/10.1029/GM121p0277

Keir, D., & Hammond, J. O. S. (2009). AFAR0911 [Dataset]. International Federation of Digital Seismograph Networks. https://doi.org/10.7914/SN/2H_2009

Keir, D., Kendall, & Ayele (2016). Rift valley volcanism past present and future [Dataset]. International Federation of Digital Seismograph Networks. https://doi.org/10.7914/SN/Y6_2016

Kennett, B. L. N., Engdahl, E. R., & Buland, R. (1995). Constraints on seismic velocities in the Earth from traveltimes. *Geophysical Journal International*, *122*(1), 108–124. https://doi.org/10.1111/j.1365-246X.1995.tb03540.x

Keranen, K. (2013). Exploring extensional tectonics beyond the Ethiopian Rift [Dataset]. International Federation of Digital Seismograph Networks. https://doi.org/10.7914/SN/YY_2013

Khoza, T. D., Jones, A. G., Muller, M. R., Evans, R. L., Miensopust, M. P., & Webb, S. J. (2013). Lithospheric structure of an Archean craton and adjacent mobile belt revealed from 2-D and 3-D inversion of magnetotelluric data: Example from southern Congo craton in northern Namibia. *Journal of Geophysical Research: Solid Earth*, *118*(8), 4378–4397. https://doi.org/10.1002/jgrb.50258

Kind, R. (1998). Namibia [Dataset]. GFZ Data Services. https://doi.org/10.14470/KP6443475642
Koelemeijer, P., Ritsema, J., Deuss, A., & van Heijst, H.-J. (2016). SP12RTS: A degree-12 model of shear- and compressional-wave velocity for Earth's mantle. *Geophysical Journal International*, *204*(2), 1024–1039. https://doi.org/10.1093/gji/ggv481
Kukla, P. A., & Stanistreet, I. G. (1991). Record of the Damaran Khomas Hochland accretionary prism in central Namibia: Refutation of an "ensialic" origin of aLate Proterozoic orogenic belt. *Geology*, *19*(5), 473. https://doi.org/10.1130/0091-7613(1991)019<0473:ROTDKH>2.3.CO;2
Laske, G., Masters, G., Ma, Z., & Pasyanos, M. E. (2012). CRUST1.0: An updated global model of Earth's crust. In *Geophysical research abstracts* (Vol. 14). Retrieved from https://meetingorganizer.copernicus.org/EGU2012/EGU2012-3743-1.pdf
Lehmann, J., Saalmann, K., Naydenov, K. V., Milani, L., Belyanin, G. A., Zwingmann, H., et al. (2016). Structural and geochronological constraints on the Pan-African tectonic evolution of the northern Damara Belt, Namibia. *Tectonics*, *35*(1), 103–135. https://doi.org/10.1002/2015TC003899
Leroy, S. (2003). DHOFAR seismic experiment [Dataset]. International Federation of Digital Seismograph Networks. https://doi.org/10.7914/SN/XZ_2003
Leseane, K., Atekwana, E. A., Mickus, K. L., Abdelsalam, M. G., Shemang, E. M., & Atekwana, E. A. (2015). Thermal perturbations beneath the incipient Okavango Rift Zone, northwest Botswana. *Journal of Geophysical Research: Solid Earth*, *120*(2), 1210–1228. https://doi.org/10.1002/2014JB011029
Levander, A., Humphreys, G., & Ryan, P. (2009). Program to investigate convective Alboran sea system overturn [Dataset]. International Federation of Digital Seismograph Networks. https://doi.org/10.7914/SN/XB_2009
Levèque, J.-J. (2010). Horn of Africa (Ethiopa, Yemen) broad-band experiment (Horn of Africa, RESIF-SISMOB) [Dataset]. RESIF - Réseau Sismologique et géodésique Français. https://doi.org/10.15778/RESIF.YR1999
Li, C., van der Hilst, R. D., Engdahl, E. R., & Burdick, S. (2008). A new global model for P wave speed variations in Earth's mantle. *Geochemistry, Geophysics, Geosystems*, *9*(5). https://doi.org/10.1029/2007GC001806
Li, C., van der Hilst, R. D., & Toksöz, M. N. (2006). Constraining P-wave velocity variations in the upper mantle beneath Southeast Asia. *Physics of the Earth and Planetary Interiors*, *154*(2), 180–195. https://doi.org/10.1016/j.pepi.2005.09.008
Li, Z. X., Bogdanova, S. V., Collins, A. S., Davidson, A., De Waele, B., Ernst, R. E., et al. (2008). Assembly, configuration, and break-up history of Rodinia: A synthesis. *Precambrian Research*, *160*(1–2), 179–210. https://doi.org/10.1016/j.precamres.2007.04.021
Lithgow-Bertelloni, C., & Silver, P. G. (1998). Dynamic topography, plate driving forces and the African superswell. *Nature*, *395*(6699), 269–272. https://doi.org/10.1038/26212
Lu, C., Grand, S. P., Lai, H., & Garnero, E. J. (2019). TX2019slab: A new P and S tomography model incorporating subducting slabs. *Journal of Geophysical Research: Solid Earth*, *124*(11), 11549–11567. https://doi.org/10.1029/2019JB017448
Macgregor, D. S. (2020). Regional variations in geothermal gradient and heat flow across the African plate. *Journal of African Earth Sciences*, *171*, 103950. https://doi.org/10.1016/j.afrearsci.2020.103950
Martin, H., & Porada, H. (1977). The intracratonic branch of the Damara orogen in South West Africa I. Discussion of geodynamic models. *Precambrian Research*, *5*(4), 311–338. https://doi.org/10.1016/0301-9268(77)90039-0
MedNet Project Partner Institutions. (1990). Mediterranean very broadband seismographic network (MedNet) [Dataset]. Istituto Nazionale di Geofisica e Vulcanologia (INGV). https://doi.org/10.13127/SD/FBBBTDTD6Q
Miller, R. M. (2008). *The geology of Namibia* (Vol. 1). Ministry of Mines and Energy, Geological Survey Windhoek.
Miller, R. M., Frimmel, H. E., & Will, T. M. (2009). Chapter 5.8 geodynamic synthesis of the Damara Orogen Sensu Lato. *Developments in Precambrian Geology*, *16*(Issue C), 231–235. https://doi.org/10.1016/S0166-2635(09)01617-X
Modisi, M. P., Atekwana, E. A., Kampunzu, A. B., & Ngwisanyi, T. H. (2000). Rift kinematics during the incipient stages of continental extension: Evidence from the nascent Okavango rift basin, northwest Botswana. *Geology*, *28*(10), 939. https://doi.org/10.1130/0091-7613(2000)28<939:RKDTIS>2.0.CO;2
Montelli, R., Nolet, G., Dahlen, F. A., & Masters, G. (2006). A catalogue of deep mantle plumes: New results from finite-frequency tomography. *Geochemistry, Geophysics, Geosystems*, *7*(11). https://doi.org/10.1029/2006GC001248
Montelli, R., Nolet, G., Masters, G., Dahlen, F. A., & Hung, S. H. (2004). Global P and PP traveltime tomography: Rays versus waves. *Geophysical Journal International*, *158*(2), 637–654. https://doi.org/10.1111/j.1365-246X.2004.02346.x
Moore, A. E., & Larkin, P. A. (2001). Drainage evolution in south-central Africa since the breakup of Gondwana. *South African Journal of Geology*, *104*(1), 47–68. https://doi.org/10.2113/104.1.47
Mulibo, G. D., & Nyblade, A. A. (2013). The P and S wave velocity structure of the mantle beneath eastern Africa and the African superplume anomaly. *Geochemistry, Geophysics, Geosystems*, *14*(8), 2696–2715. https://doi.org/10.1002/ggge.20150
Ni, S., & Helmberger, D. V. (2003). Seismological constraints on the South African superplume; could be the oldest distinct structure on Earth. *Earth and Planetary Science Letters*, *206*(1–2), 119–131. https://doi.org/10.1016/S0012-821X(02)01072-5
Ni, S., Tan, E., Gurnis, M., & Helmberger, D. (2002). Sharp sides to the African superplume. *Science*, *296*(5574), 1850–1852. https://doi.org/10.1126/science.1070698
Nyblade, A. A. (2000). Seismic investigation of deep structure beneath the Ethiopian plateau and Afar depression [Dataset]. International Federation of Digital Seismograph Networks. https://doi.org/10.7914/SN/XI_2000
Nyblade, A. A. (2007). Africa array- Uganda/Tanzania [Dataset]. International Federation of Digital Seismograph Networks. https://doi.org/10.7914/SN/ZP_2007
Nyblade, A. A. (2010). AfricaArray SE Tanzania basin experiment [Dataset]. International Federation of Digital Seismograph Networks. https://doi.org/10.7914/SN/YH_2010
Nyblade, A. A. (2015a). AfricaArray - Namibia [Dataset]. IRIS. https://doi.org/10.7914/SN/8A_2015
Nyblade, A. A. (2015b). REU: Imaging the Bushveld complex, South Africa [Dataset]. International Federation of Digital Seismograph Networks. https://doi.org/10.7914/SN/ZT_2015
Nyblade, A. A. (2017). Broadband seismic experiment in NE Uganda to investigate plume-lithosphere interactions [Dataset]. International Federation of Digital Seismograph Networks. https://doi.org/10.7914/SN/XW_2017
Nyblade, A. A., Dirks, P., Durrheim, R., Webb, S., Jones, M., Cooper, G., & Graham, G. (2008). AfricaArray: Developing a geosciences workforce for Africa's natural resource sector. *The Leading Edge*, *27*(10), 1358–1361. https://doi.org/10.1190/1.2996547
Nyblade, A. A., Pollack, H. N., Jones, D. L., Podmore, F., & Mushayandebvu, M. (1990). Terrestrial heat flow in east and southern Africa. *Journal of Geophysical Research*, *95*(B11), 17371–17384. https://doi.org/10.1029/JB095iB11p17371
Nyblade, A. A., & Robinson, S. W. (1994). The African superswell. *Geophysical Research Letters*, *21*(9), 765–768. https://doi.org/10.1029/94GL00631

O'Donnell, J. P., Adams, A., Nyblade, A. A., Mulibo, G. D., & Tugume, F. (2013). The uppermost mantle shear velocity structure of eastern Africa from Rayleigh wave tomography: Constraints on rift evolution. *Geophysical Journal International*, *194*(2), 961–978. https://doi.org/10.1093/gji/ggt135

Ortiz, K., Nyblade, A. A., van der Meijde, M., Paulssen, H., Kwadiba, M., Ntibinyane, O., et al. (2019). Upper mantle P and S wave velocity structure of the Kalahari Craton and surrounding Proterozoic terranes, southern Africa. *Geophysical Research Letters*, *46*(16), 9509–9518. https://doi.org/10.1029/2019GL084053

Owens, T., & Nyblade, A. A. (1994). Seismic investigations of the lithospheric structure of the Tanzanian Craton [Dataset]. International Federation of Digital Seismograph Networks. https://doi.org/10.7914/SN/XD_1994

Owens, T. J., Nyblade, A. A., Gurrola, H., & Langston, C. A. (2000). Mantle transition zone structure beneath Tanzania, East Africa. *Geophysical Research Letters*, *27*(6), 827–830. https://doi.org/10.1029/1999gl005429

Paige, C. C., & Saunders, M. A. (1982). Algorithm 583: LSQR: Sparse linear equations and least squares problems. *ACM Transactions on Mathematical Software*, *8*(2), 195–209. https://doi.org/10.1145/355993.356000

Pandey, S., Yuan, X., Debayle, E., Geissler, W. H., & Heit, B. (2022). Plume-lithosphere interaction beneath southwestern Africa – Insights from multi-mode Rayleigh wave tomography. *Tectonophysics*, *842*, 229587. https://doi.org/10.1016/j.tecto.2022.229587

Passchier, C., Trouw, R., & da Silva Schmitt, R. (2016). How to make a transverse triple junction-New evidence for the assemblage of Gondwana along the Kaoko-Damara Belts, Namibia. *Geology*, *44*(10), 843–846. https://doi.org/10.1130/G38015.1

Pastier, A. M., Dauteuil, O., Murray-Hudson, M., Moreau, F., Walpersdorf, A., & Makati, K. (2017). Is the Okavango Delta the terminus of the East African Rift System? Towards a new geodynamic model: Geodetic study and geophysical review. *Tectonophysics*, *712*, 469–481. https://doi.org/10.1016/j.tecto.2017.05.035

Pavlis, G. L., & Vernon, F. L. (2010). Array processing of teleseismic body waves with the USArray. *Computers & Geosciences*, *36*(7), 910–920. https://doi.org/10.1016/j.cageo.2009.10.008

Penn State University. (2004). AfricaArray [Dataset]. International Federation of Digital Seismograph Networks. https://doi.org/10.7914/SN/AF

Peyve, A. A. (2011). Seamounts in the East of south Atlantic: Origin and correlation with Mesozoic-Cenozoic magmatic structures of West Africa. *Geotectonics*, *45*(3), 195–209. https://doi.org/10.1134/S0016852111030058

Pik, R., Deniel, C., Coulon, C., Yirgu, G., Hofmann, C., & Ayalew, D. (1998). The northwestern Ethiopian plateau flood basalts: Classification and spatial distribution of magma types. *Journal of Volcanology and Geothermal Research*, *81*(1–2), 91–111. https://doi.org/10.1016/S0377-0273(97)00073-5

Porada, H. (1979). The Damara-Ribeira Orogen of the Pan-Africanbrasiliano cycle in Namibia (Southwest Africa) and Brazil as interpreted in terms of continental collision. *Tectonophysics*, *57*(2–4), 237–265. https://doi.org/10.1016/0040-1951(79)90150-1

Priestley, K., Mckenzie, D., Debayle, E., & Pilidou, S. (2008). The African upper mantle and its relationship to tectonics and surface geology. *Geophysical Journal International*, *175*(3), 1108–1126. https://doi.org/10.1111/j.1365-246X.2008.03951.x

Rajaonarison, T. A., Stamps, D. S., Naliboff, J., Nyblade, A., & Njinju, E. A. (2023). A geodynamic investigation of plume-lithosphere interactions beneath the East African rift. *Journal of Geophysical Research: Solid Earth*, *128*(4). https://doi.org/10.1029/2022JB025800

Rawlinson, N., Fichtner, A., Sambridge, M., & Young, M. K. (2014). Seismic tomography and the assessment of uncertainty. *Advances in Geophysics*, *55*, 1–76. https://doi.org/10.1016/BS.AGPH.2014.08.001

Ritsema, J., Heijst, H. J. V., & Woodhouse, J. H. (1999). Complex shear wave velocity structure imaged beneath Africa and Iceland. *Science*, *286*(5446), 1925–1928. https://doi.org/10.1126/science.286.5446.1925

Ritsema, J., Nyblade, A. A., Owens, T. J., Langston, C. A., & VanDecar, J. C. (1998). Upper mantle seismic velocity structure beneath Tanzania, East Africa: Implications for the stability of Cratonic lithosphere. *Journal of Geophysical Research*, *103*(B9), 21201–21213. https://doi.org/10.1029/98jb01274

Roult, G., Montagner, J. P., Romanowicz, B., Cara, M., Rouland, D., Pillet, R., et al. (2010). The GEOSCOPE Program: Progress and challenges during the past 30 years. *Seismological Research Letters*, *81*(3), 427–452. https://doi.org/10.1785/gssrl.81.3.427

Saeidi, H., Hansen, S. E., & Nyblade, A. A. (2023). Deep mantle influence on the Cameroon volcanic line. *Geochemistry, Geophysics, Geosystems*, *24*(1). https://doi.org/10.1029/2022GC010621

San Fernando Royal Naval Observatory (ROA), Universidad Complutense De Madrid (UCM), Helmholtz-Zentrum Potsdam Deutsches GeoForschungsZentrum (GFZ), Universidade De Évora (UEVORA Portugal), & Institute Scientifique Of Rabat (ISRABAT Morocco). (1996). The Western Mediterranean BB seismic network [Dataset]. Deutsches GeoForschungsZentrum GFZ. https://doi.org/10.14470/JZ581150

Sarafian, E., Evans, R. L., Abdelsalam, M. G., Atekwana, E., Elsenbeck, J., Jones, A. G., & Chikambwe, E. (2018). Imaging Precambrian lithospheric structure in Zambia using electromagnetic methods. *Gondwana Research*, *54*, 38–49. https://doi.org/10.1016/j.gr.2017.09.007

Scripps Institution of Oceanography. (1986). Global seismograph network - IRIS/IDA [Dataset]. International Federation of Digital Seismograph Networks. https://doi.org/10.7914/SN/II

Silver, P. (1997). Anatomy of an Archean craton, South Africa, A multidisciplinary experiment across the Kaapvaal Craton [Dataset]. International Federation of Digital Seismograph Networks. https://doi.org/10.7914/SN/XA_1997

Simmons, N. A., Forte, A. M., Boschi, L., & Grand, S. P. (2010). GyPSuM: A joint tomographic model of mantle density and seismic wave speeds. *Journal of Geophysical Research*, *115*(B12), B12310. https://doi.org/10.1029/2010JB007631

Simmons, N. A., Myers, S. C., Johannesson, G., & Matzel, E. (2012). LLNL-G3Dv3: Global P wave tomography model for improved regional and teleseismic travel time prediction. *Journal of Geophysical Research*, *117*(B10). https://doi.org/10.1029/2012JB009525

Sleep, N. H., Ebinger, C. J., & Kendall, J. M. (2002). Deflection of mantle plume material by cratonic keels. *Geological Society, London, Special Publications*, *199*(1), 135–150. https://doi.org/10.1144/GSL.SP.2002.199.01.08

Sun, M., Fu, X., Liu, K. H., & Gao, S. S. (2018). Absence of thermal influence from the African Superswell and cratonic keels on the mantle transition zone beneath southern Africa: Evidence from receiver function imaging. *Earth and Planetary Science Letters*, *503*, 108–117. https://doi.org/10.1016/j.epsl.2018.09.012

Tesoniero, A., Auer, L., Boschi, L., & Cammarano, F. (2015). Hydration of marginal basins and compositional variations within the continental lithospheric mantle inferred from a new global model of shear and compressional velocity. *Journal of Geophysical Research: Solid Earth*, *120*(11), 7789–7813. https://doi.org/10.1002/2015JB012026

Thomas, C. (2010). Morocco-Muenster [Dataset]. International Federation of Digital Seismograph Networks. https://doi.org/10.7914/SN/3D_2010

Tilmann, F., Yuan, X., Rümpker, G., & Rindraharisaona, E. (2012). SELASOMA project, Madagascar 2012-2014 [Dataset]. GFZ Data Services. https://doi.org/10.14470/MR7567431421

To, A., Romanowicz, B., Capdeville, Y., & Takeuchi, N. (2005). 3D effects of sharp boundaries at the borders of the African and Pacific Superplumes: Observation and modeling. *Earth and Planetary Science Letters*, *233*(1–2), 137–153. https://doi.org/10.1016/j.epsl.2005.01.037

Utrecht University (UU Netherlands). (1983). NARS [Dataset]. International Federation of Digital Seismograph Networks. https://doi.org/10.7914/SN/NR

Velasco, A., Kaip, G., Wamalwa, A., & Patlan, E. (2011). Seismic characterization of Menengai Crater, Kenya [Dataset]. International Federation of Digital Seismograph Networks. https://doi.org/10.7914/SN/1C_2011

Vergne, J., Doubre, C., & Leroy, S. (2014). Seismic network 7C:Dora experiment (RESIF-SISMOB) [Dataset]. RESIF - Réseau Sismologique et géodésique Français. https://doi.org/10.15778/RESIF.7C2009

Wessel, P., Smith, W. H. F., Scharroo, R., Luis, J., & Wobbe, F. (2013). Generic mapping tools: Improved version released [Software]. Eos, Transactions American Geophysical Union, *94*(45), 409–410. https://doi.org/10.1002/2013EO450001

Weston, J., Engdahl, E. R., Harris, J., Di Giacomo, D., & Storchak, D. A. (2018). ISC-EHB: Reconstruction of a robust earthquake data set. *Geophysical Journal International*, *214*(1), 474–484. https://doi.org/10.1093/gji/ggy155

White-Gaynor, A. L., Nyblade, A. A., Durrheim, R., Raveloson, R., Meijde, M., Fadel, I., et al. (2020). Lithospheric boundaries and upper mantle structure beneath southern Africa imaged by P and S wave velocity models. *Geochemistry, Geophysics, Geosystems*, *21*(10). https://doi.org/10.1029/2020GC008925

White-Gaynor, A. L., Nyblade, A. A., Durrheim, R. J., Raveloson, R., van der Meijde, M., Fadel, I., et al. (2021). Shear-wave velocity structure of the southern African upper mantle: Implications for craton structure and plateau uplift. *Geophysical Research Letters*, *48*(7). https://doi.org/10.1029/2020GL091624

Wiens, D. A., & Nyblade, A. A. (2005). Broadband seismic investigation of the Cameroon volcanic line [Dataset]. International Federation of Digital Seismograph Networks. https://doi.org/10.7914/SN/XB_2005

Wookey, J., Horleston, A., Di Leo, J., Thomas, C., Harnafi, M., & Elouai, D. (2011). CoMITAC Morocco-Bristol network [Dataset]. International Federation of Digital Seismograph Networks. https://doi.org/10.7914/SN/ZI_2011

Wysession, M., Wiens, D. A., & Nyblade, A. A. (2011). Investigation of sources of intraplate volcanism using Passcal broadband instruments in Madagascar, the Comores, and Mozambique [Dataset]. International Federation of Digital Seismograph Networks. https://doi.org/10.7914/SN/XV_2011

Yu, Y., Gao, S. S., & Liu, K. H. (2020). Topography of the 410 and 660 km discontinuities beneath the Cenozoic Okavango Rift Zone and adjacent Precambrian provinces. *Journal of Geophysical Research: Solid Earth*, *125*(9), 1–14. https://doi.org/10.1029/2019JB019290

Yu, Y., Gao, S. S., Moidaki, M., Reed, C. A., & Liu, K. H. (2015). Seismic anisotropy beneath the incipient Okavango rift: Implications for rifting initiation. *Earth and Planetary Science Letters*, *430*, 1–8. https://doi.org/10.1016/j.epsl.2015.08.009

Yu, Y., Liu, K. H., Huang, Z., Zhao, D., Reed, C. A., Moidaki, M., et al. (2017). Mantle structure beneath the incipient Okavango rift zone in southern Africa. *Geosphere*, *13*(1), 102–111. https://doi.org/10.1130/GES01331.1

Yu, Y., Liu, K. H., Reed, C. A., Moidaki, M., Mickus, K., Atekwana, E. A., & Gao, S. S. (2015b). A joint receiver function and gravity study of crustal structure beneath the incipient Okavango Rift, Botswana. *Geophysical Research Letters*, *42*(20), 8398–8405. https://doi.org/10.1002/2015GL065811

Yuan, Q., & Li, M. (2022). Instability of the African large low-shear-wave-velocity province due to its low intrinsic density. *Nature Geoscience*, *15*(4), 334–339. https://doi.org/10.1038/s41561-022-00908-3

References From the Supporting Information

Amaru, M. L. (2007). *Global travel time tomography with 3-D reference models* (Doctoral thesis). Utrecht University.

Burdick, S., van der Hilst, R. D., Vernon, F. L., Martynov, V., Cox, T., Eakins, J., et al. (2012). Model update March 2011: Upper mantle heterogeneity beneath north America from traveltime tomography with global and USArray transportable array data. *Seismological Research Letters*, *83*(1), 23–28. https://doi.org/10.1785/gssrl.83.1.23

Obayashi, M., Yoshimitsu, J., Nolet, G., Fukao, Y., Shiobara, H., Sugioka, H., et al. (2013). Finite frequency whole mantle P wave tomography: Improvement of subducted slab images. *Geophysical Research Letters*, *40*(21), 5652–5657. https://doi.org/10.1002/2013GL057401

Sigloch, K. (2011). Mantle provinces under North America from multifrequency *P* wave tomography. *Geochemistry, Geophysics, Geosystems*, *12*(2). https://doi.org/10.1029/2010GC003421

Tsekhmistrenko, M., Sigloch, K., Hosseini, K., & Barruol, G. (2021). A tree of Indo-African mantle plumes imaged by seismic tomography. *Nature Geoscience*, *14*(8), 612–619. https://doi.org/10.1038/s41561-021-00762-9